Global and Planetary Change 211 (2022) 103790

Contents lists available at ScienceDirect

Global and Planetary Change

journal homepage: www.elsevier.com/locate/gloplacha

Accounting for atmospheric carbon dioxide variations in pollen-based reconstruction of past hydroclimates

I. Colin Prentice [a,*], Roberto Villegas-Diaz [b], Sandy P. Harrison [b]

[a] Georgina Mace Centre for the Living Planet, Department of Life Sciences, Imperial College London, Silwood Park Campus, Buckhurst Road, Ascot SL5 7PY, UK
[b] Geography & Environmental Sciences, Reading University, Whiteknights, Reading, RG6 6AH, UK

ARTICLE INFO

Editor: Jed O Kaplan

Keywords:
Water-use efficiency
Moisture index
Palaeoclimate reconstructions
Glacial climate
Eco-evolutionary optimality

ABSTRACT

Changes in atmospheric carbon dioxide (CO_2) concentration directly influence the ratio of stomatal water loss to carbon uptake. This ratio (e) is a fundamental quantity for terrestrial ecosystems, as it defines the water requirement for plant growth. Statistical and analogue-based methods used to reconstruct past hydroclimate variables from fossil pollen assemblages do not take account of the effect of CO_2 variations on e. Here we present a general, globally applicable method to correct for this effect. The method involves solving an equation that relates e to a climatic moisture index (MI, the ratio of mean annual precipitation to mean annual potential evapotranspiration), mean growing-season temperature, and ambient CO_2. The equation is based on the least-cost optimality hypothesis, which predicts how the ratio (χ) of leaf-internal to ambient CO_2 varies with vapour pressure deficit (vpd), growing-season temperature and atmospheric pressure, combined with experimental evidence on the response of χ to the CO_2 level at which plants have been grown. An empirical relationship based on global climate data is used to relate vpd to MI and growing-season temperature. The solution to the equation allows past MI to be estimated from pollen-reconstructed MI, given past CO_2 and temperature. This MI value can be used to estimate mean annual precipitation, accounting for the effects of orbital variations, temperature and cloud cover (inferred from MI) on potential evapotranspiration. A pollen record from semi-arid Spain that spans the last glacial interval is used to illustrate the method. Low CO_2 leads to estimated MI being larger than reconstructed MI during glacial times. The CO_2 effect on inferred precipitation was partly offset by increased cloud cover; nonetheless, inferred precipitation was greater than present almost throughout the glacial period. This method allows a more robust reconstruction of past hydroclimatic variations than currently available tools.

1. Introduction

CO_2 uptake through stomata during photosynthesis means that carbon assimilation by plants is unavoidably accompanied by water loss. When ambient CO_2 is high, water-use efficiency (the amount of water lost per unit carbon assimilated) is high or, conversely, the water loss required to achieve a unit of CO_2 assimilation (here denoted e) is low. e is a fundamental quantity for land ecosystems, as it defines the amount of water required for the growth of plants. All else equal, low e implies higher vegetation productivity and cover for a given supply of water. High e implies lower vegetation productivity and cover for the same supply of water. Increases in water-use efficiency due to the recent CO_2 rise are well documented by comparisons of measured CO_2 and latent heat fluxes, and by trends in stable carbon isotope discrimination (Keenan et al., 2013; Dekker et al., 2016). This effect also provides part of the explanation for recent global greening (Piao et al., 2006; Zhu et al., 2016; Haverd et al., 2020) and widespread increases in woody plant cover (Eamus and Palmer, 2007; Archer et al., 2017). The converse situation prevailed during intervals of low CO_2, including the last glacial interval (115 to 11.7 kyr). Thus, glacial-age palaeodata indicating open, treeless vegetation characteristic of dry climates today do not necessarily imply low water availability in the past because, in principle, low CO_2 alone could have been responsible for the apparent dryness. Indeed, vegetation-model experiments have indicated that the impacts of low CO_2 on vegetation structure and composition during glacial times were at least as great as the impacts of the glacial climate (Jolly and Haxeltine, 1997; Harrison and Prentice, 2003; Bragg et al., 2013; Martin Calvo and Prentice, 2015), resulting inter alia in a global reduction of

* Corresponding author.
E-mail address: c.prentice@imperial.ac.uk (I.C. Prentice).

https://doi.org/10.1016/j.gloplacha.2022.103790
Received 4 August 2021; Received in revised form 6 March 2022; Accepted 16 March 2022
Available online 19 March 2022
0921-8181/© 2022 The Authors. Published by Elsevier B.V. This is an open access article under the CC BY license (http://creativecommons.org/licenses/by/4.0/).

primary production and forest cover (Harrison and Prentice, 2003; Prentice et al., 2011).

Methods are therefore needed to quantify the expected effect of CO_2 changes, to avoid potentially biased estimation of past hydroclimates at CO_2 levels different from those prevalent during the calibration period. Although the impacts of low CO_2 on plant function have been known for decades (Solomon, 1984; Idso, 1989; Polley et al., 1993; Farquhar, 1997; Cowling and Sykes, 1999), there have been few attempts to incorporate this concept into the quantitative climatic interpretation of past vegetation changes. Statistical and modern-analogue methods to reconstruct past hydroclimates from pollen data depend on relationships between pollen abundances and climate variables that are determined under recent atmospheric conditions (Chevalier et al., 2020). They cannot, by their nature, take the effect of varying CO_2 into account. Process-based vegetation models that incorporate CO_2 impacts on plant growth can be inverted to make climate reconstructions that do take account of variable CO_2 (e.g. Guiot et al., 2000; Wu et al., 2007; Izumi and Bartlein, 2016). Published model inversions for palaeo-climate variables have used variants of the same equilibrium vegetation model (BIOME3: Haxeltine and Prentice, 1996; BIOME4: Kaplan et al., 2003; BIOME5beta: Izumi and Bartlein, 2016) and also a dynamic global vegetation model, LPJ-GUESS (Garreta et al., 2010; 2012). However, inversion results depend on the particularities of the vegetation model (Chevalier et al., 2020). Comparisons of model predictions of vegetation responses to future CO_2 changes have shown that this sensitivity is not well constrained, and differs between models (Friedlingstein et al., 2019; Arora et al., 2020) – motivating the development of simpler and more robust methods.

We previously described a prototype method to correct statistical reconstructions of a standard moisture index (Prentice et al., 2017). This method has been applied to reconstruct CO_2-corrected changes in moisture availability at the Last Glacial Maximum globally (Cleator et al., 2020) and through the last glacial cycle at El Cañizar de Villarquemado, a site in semi-arid Spain (Wei et al., 2021). Here we introduce a major update of the method. The updated method is simpler, and requires fewer assumptions, than the originally published method. When empirical relationships among climate variables are required, they are based on new analyses of global climate data. The method is based on a combination of eco-evolutionary optimality theory and published experimental findings on how the ratio (χ) of leaf-internal to ambient CO_2 responds to variations in ambient CO_2. We show how this method can be applied to statistical or analogue-based reconstructions of past values of the moisture index (MI), defined as the ratio of mean annual precipitation (MAP) to mean annual potential evapotranspiration (PET). We also show how past precipitation can be estimated from CO_2-corrected MI, taking into account orbital variations (affecting the seasonal and latitudinal distribution of insolation), temperature and cloud cover (estimated from an empirical relationship to MI). The method is illustrated using the pollen data from El Cañizar de Villarquemado.

2. Methods

2.1. Description of the model

The model relies on the interdependencies of several climatic variables, and on the control of stomatal behaviour by climate, atmospheric pressure (primarily determined by elevation) and atmospheric CO_2, as illustrated in Fig. 1. The following text explains each of these relationships and indicates how they are used.

Fick's law describes both the diffusion of CO_2 into leaves and the diffusion of water out of leaves through stomata:

$$A = g_s\, c_a\, (1-\chi)/P \quad (1)$$

$$E = 1.6\, g_s\, D/P \quad (2)$$

where A is carbon assimilation, E is water loss, g_s is stomatal conductance to CO_2, c_a is the ambient partial pressure of CO_2, χ is the ratio of leaf-internal to ambient CO_2, P is atmospheric pressure and D is vapour pressure deficit (vpd). The factor 1.6 arises because of the different molecular diffusivities of CO_2 and water. A, E and g_s here all have units of mol m^{-2} s^{-1} while c_a, D and P have units of Pa; hence both are normalized by atmospheric pressure, converting them to mole fractions in eqs. (1) and (2). Dividing (2) by (1) leads to a notably simple expression for e, the ratio (E/A) of water loss to CO_2 uptake:

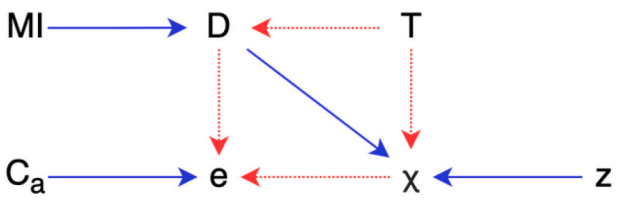

Fig. 1. Environmental influences on water loss per unit carbon gain (e). MI, moisture index; D, vapour pressure deficit; T, temperature; c_a, ambient mole fraction of CO_2; χ, ratio of leaf-internal to ambient CO_2; z, elevation. Blue arrows indicate a negative influence, red arrows a positive influence. (For interpretation of the references to colour in this figure legend, the reader is referred to the web version of this article.)

$$e = 1.6\, D/\{c_a\, (1-\chi)\} \quad (3)$$

Here e is the reciprocal of water use efficiency, a fundamental quantity describing the balance betwen CO_2 uptake and water loss at the leaf level. The key hypothesis underlying our CO_2 correction is that vegetation structure and composition respond to changes in this balance (Prentice et al., 2017; Gonsamo et al., 2021) rather than to any variable derived solely from meteorological data, including MI, that does not take plant physiological effects of c_a into account.

The following equation, introduced by Prentice et al. (2017) with slightly different notation, summarizes how the CO_2 correction is implemented:

$$e\,(T_1, \mathrm{MI}_1, c_{a1}) = e\,(T_0, \mathrm{MI}_0, c_{a0}) \quad (4)$$

where T_1 is the past growing-season mean temperature (reconstructed), MI_1 is the "true" past value of MI (to be estimated), c_{a1} is the past atmospheric CO_2 (known), T_0 is the recent growing-season mean temperature, MI_0 is the reconstructed past value of MI, and c_{a0} is the recent atmospheric CO_2. This equation states that the "true" past MI is the value that would produce the same e (under past atmospheric conditions) that the reconstructed past MI produces under recent atmospheric conditions, i.e. those pertaining to the modern pollen calibration data set. The indices (0,1) link variables that belong together, i.e. on either the left-hand (1) or the right-hand (0) side of eq. (4).

It is assumed that a reconstruction of past growing-season mean temperature is available. Defining the growing season conventionally as the period of the year with climatological temperatures >0 °C, and approximating the seasonal cycle of temperatures by a sine curve, it is possible to obtain such a reconstruction from alternative reconstructed variables such as growing degree days and coldest-month temperatures, or December–January-February (DJF) and June–July-August (JJA) temperatures. See section 2.2 below for an example.

Equation (4) also assumes that the reconstructed temperature, unlike MI, is not biased by CO2. This point is taken up again in the Discussion. However, the potential influence of cha.

We now introduce the main innovation in this paper, which is the use of vpd as a key intermediate variable in the CO_2 correction model (Fig. 1). We rely on a new empirical equation based on global climate data (Appendix 1) that allows vpd to be estimated from MI. Eq. (4) then reduces to the following simple form:

$$D_1/\{c_{a1}\, (1-\chi_1)\} = D_0/\{c_{a0}\, (1-\chi_0)\} \quad (5)$$

where D_1 and χ_1 are past values, and D_0 and χ_0 are present values.

Prentice et al. (2014) showed that the least-cost hypothesis, an eco-evolutionary optimality hypothesis based on the idea that plants minimize the combined costs (per unit carbon assimilation) of maintaining the biochemical and water-transport capacities required for photosynthesis, explicitly predicts variations in χ as a function of climate, with vpd, temperature and atmospheric pressure as the major controls. This hypothesis has now been extensively validated using global compilations of stable carbon isotope data on leaves (Wang et al., 2017) and wood (Lavergne et al., 2020a). Variations in optimal χ with temperature, vpd and atmospheric pressure conform to the following relationship:

$$1-\chi = (1-\Gamma^*/c_a)\sqrt{D}/(\xi+\sqrt{D}) \quad (6)$$

where Γ^* is the photorespiratory compensation point (dependent on temperature and atmospheric pressure), and.

$$\xi = \sqrt{\{\beta\,(K+\Gamma^*)/(1.6\,\eta^*)\}} \quad (7)$$

where β is a dimensionless constant estimated as 146 based on modern stable carbon isotope data (Stocker et al., 2020), K is the effective Michaelis-Menten coefficient of Rubisco (in Pa; dependent on temperature and atmospheric pressure), and η^* is the viscosity of water relative to its value at 25 °C (dimensionless; dependent on temperature). Experiments in which plants were grown under otherwise constant environmental conditions at a wide range of CO_2 levels (Schubert and Jahren, 2012) have shown that χ also varies predictably as a function of c_a. This finding has received further support from analyses of changes in leaf-level stable carbon isotope discrimination since the last glacial period (Schubert and Jahren, 2015; Voelker et al., 2016). The CO_2 response presented by Schubert and Jahren (2012) can be expressed in a simplified way as:

$$\chi = c_a/(c_a+\omega) \quad (8)$$

where $\omega = 9.7$ Pa (see Appendix 2 for derivation). Combining eqs. (7) and (8) gives:

$$c_a\,(1-\chi) = \{\omega\,(c_a-\Gamma^*)/(c_a+\omega)\}\sqrt{D}/(\xi+\sqrt{D}) \quad (9)$$

Equation (5) can now be represented as a quadratic in $\sqrt{D_1}$:

$$\xi_1\sqrt{D_1}+D_1 = \{(c_{a1}-\Gamma^*_1)/(c_{a0}-\Gamma^*_0)\}\,\{(c_{a0}+\omega)/(c_{a1}+\omega)\}\,(\xi_0\sqrt{D_0}+D_0) \quad (10)$$

where ξ_1 and ξ_0 are values of ξ calculated respectively at past (reconstructed) and present temperatures, and Γ^*_1 and Γ^*_0 are defined similarly. Eq. (10) has an analytical solution:

$$\sqrt{D_1} = -(\xi_1/2)+\sqrt{\left\{Q+(\xi_1/2)^2\right\}} \quad (11)$$

where Q is the right-hand side of eq. (10), and $\sqrt{}$ denotes the positive square root. (Note that the code used here retains the more general iterative solution method used in Prentice et al., 2017; we have shown that the result is identical.) The estimated value of $\sqrt{D_1}$ is squared to yield D_1, then D_1 is converted back to MI by inversion of the relationship from Appendix 1:

$$MI_1 = [(bT_1)-ln\,(D_1/a)]/c \quad (12)$$

where the constants a, b and c are as given in eq. (A.1.2).

If required, this revised estimate of MI can be further converted – albeit with some additional approximations – into an inferred value of MAP. From the definition of MI, MAP is obtained simply by multiplying MI with PET. PET does not depend on CO_2, so no further CO_2 effect needs to be considered. However, PET does vary with insolation, cloud cover, and temperature. Our strategy to estimate past PET makes use of the program SPLASH (Davis et al., 2017), which computes PET on a daily timestep and sums the values over the year. Daily PET is calculated by SPLASH using the Priestley-Taylor equation:

$$\lambda\,PET = \alpha_0\,R_n\,s/(s+\gamma) \quad (13)$$

where λ is the latent heat of vaporization of water, α_0 is a constant set at its canonical value of 1.26, R_n is an estimate of daily net radiation at the canopy surface (a function of insolation, cloud cover, elevation and temperature), s is the slope of the relationship between saturated vapour pressure and temperature (itself a function of temperature), and γ is the psychrometer "constant" (a function of atmospheric pressure). To estimate PET under past conditions we therefore need to provide SPLASH with information on insolation, cloud cover and temperature. The time-course of insolation for any given year can be calculated from the known variations in the Earth's orbital parameters. Cloud cover is estimated from (corrected) MI using the global empirical relationship described in Appendix 3. The time-course of temperature is estimated based on recent data for the site, modified by the differences between past (reconstructed) and recent temperatures in the coldest and warmest months. These differences are interpolated sinusoidally to the seasonal cycle.

The model has been implemented in R. The correction procedure for MI is described in detail in Supplementary Data 1. The re-calculation of PET in order to estimate past MAP is detailed in Supplementary Data 2. Fig. 2 summarizes the complete method for obtaining palaeo-estimates of both MI and MAP.

2.2. Fossil reconstructions

We applied the new approach to existing reconstructions of MI from the pollen record of El Cañizar de Villarquemado, Spain (Wei et al., 2021). The record covers the last part of Marine Isotope Stage (MIS) 6 to the Late Holocene (Valero-Garcés et al., 2019; González-Sampériz et al., 2020). The MI reconstructions were made using tolerance-weighted-averaging partial least squares regression (TWA-PLS: Liu et al., 2020). The modern pollen dataset was derived from the SPECIAL Modern Pollen Data Set (SMPDS: Harrison, 2019). The SMPDS consists of relative abundance records of pollen taxa from 6459 terrestrial sites in Europe, the Middle East and northern Eurasia. The pollen records were taxonomically standardized, and filtered to remove obligate aquatics, insectivorous species, introduced species, and taxa that only occur in cultivation. Taxa (mainly herbaceous) with only sporadic occurrences were amalgamated to higher taxonomic levels (genus, sub-family or family) after ensuring consistency with their distribution in climate space. The data set as analysed comprises data on 247 taxa.

CO_2 levels varied between 180 and 280 ppm during the interval covered by the record, and were below 240 ppm during the full glacial interval represented by MIS 4, MIS3 and MIS2. Wei et al. (2021) used the method of Prentice et al. (2017) to correct MI to account for changing CO_2 levels. Here we use the uncorrected statistical reconstructions as the starting point and apply the updated method as described above. The calculations are laid out step-by-step in Supplementary Data 3.

3. Results

The estimated MI during the glacial period at El Cañizar de Villarquemado (Fig. 3) is consistently greater than implied by the statistical reconstructions. The difference between the two estimates is, as expected, largest during intervals when CO_2 was lowest. The statistical method underestimates the corrected MI by ca 30% on average for the samples from the glacial period and by up to 80% for some individual samples. The qualitative features of our estimation of hydroclimatic changes at the site are similar to those previously published (Wei et al., 2021), although the magnitudes of the correction to MI are between 5 and 25% smaller (Fig. 3).

MAP in this region today is *ca* 380-400 mm, while the glacial-age estimates range from 490 to 760 mm (Fig. 4). Fig. 4 shows the time-course of estimated MAP after correction of PET by one factor at a time (temperature, insolation and cloud cover), and by all three factors together. The temporal patterns of estimated MAP after consideration of changes in only temperature or insolation (Fig. 4) resemble that of the

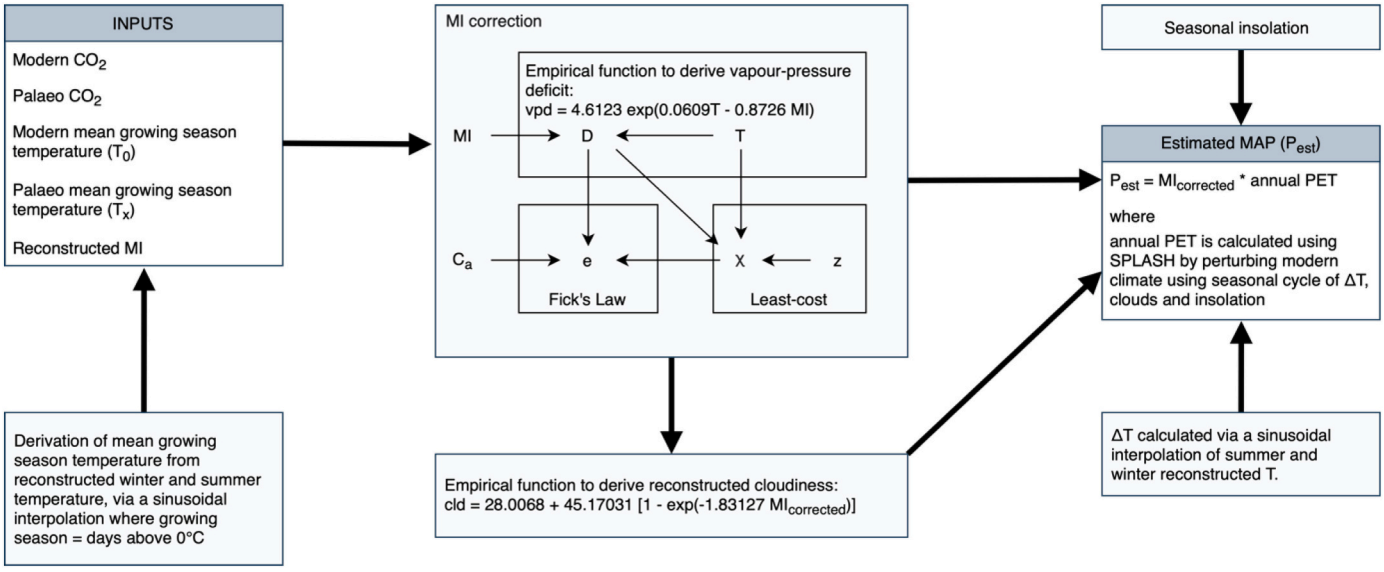

Fig. 2. Flow chart showing the procedure used to correct the moisture index (MI) and estimate mean annual precipitation (MAP) under varying atmospheric conditions.

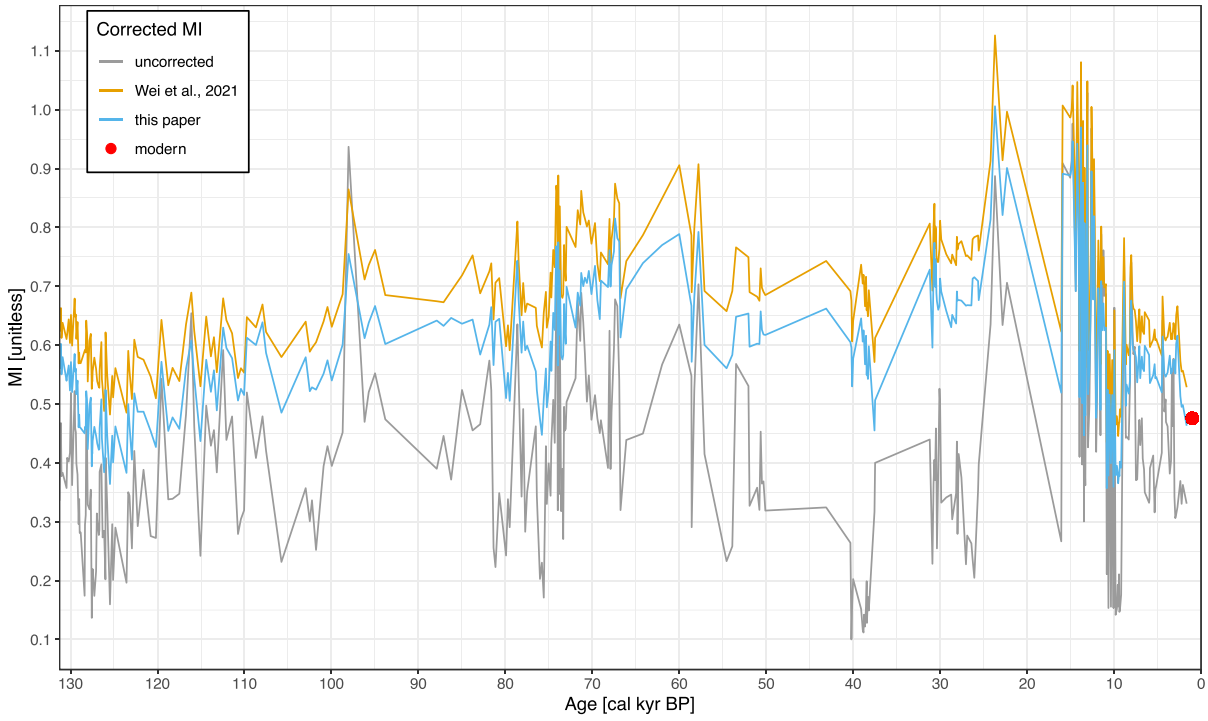

Fig. 3. Reconstructed and corrected moisture index (MI) at El Cañizar de Villarquemado from the last part of MIS 6 to the Late Holocene (131,200 to 1660 yr BP). The previously published corrected values from Wei et al. (2021) are shown for comparison. The present-day MI for the region is shown with a red dot. (For interpretation of the references to colour in this figure legend, the reader is referred to the web version of this article.)

corrected MI (Fig. 3), but the values seem implausibly high. Changes in cloud cover have a much larger (offsetting) effect, and the reconstructions of precipitation considering all three factors do not differ greatly from those considering cloud cover alone (Fig. 4). Estimated precipitation is still higher than present almost throughout the glacial period. However, the values obtained after considering cloud cover are more moderate. The key mechanism at work here is that the high reconstructed (corrected) MI values for the glacial period, which imply increased cloud cover relative to today, also imply reduced PET.

4. Discussion

Reconstruction of MI is preferred to reconstruction of mean annual precipitation from pollen data by statistical or modern-analogue techniques, because MI is closer to the environment experienced by plants: the effectiveness of precipitation in supplying water depends on PET, and therefore varies with solar radiation and growing-season temperature. However, MI does not fully describe plant-available moisture, because atmospheric CO_2 modulates its effects. This is an important issue not only for palaeoclimate reconstruction but also for projections

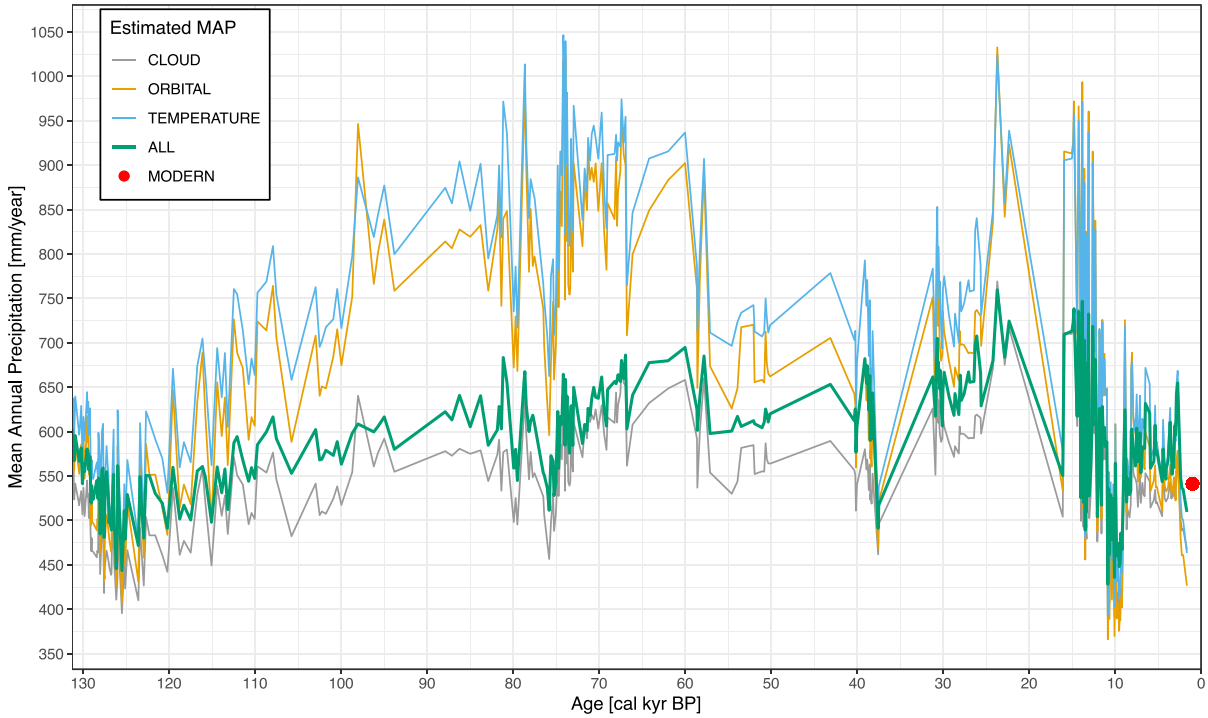

Fig. 4. Estimated mean annual precipitation (MAP) at El Cañizar de Villarquemado from the last part of MIS 6 to the Late Holocene (131,200 to 1660 yr BP), based on the corrected MI reconstructions as shown in Fig. 3, after considering the effects of changes in temperature (temperature), cloud cover (cloud), orbitally-induced changes in solar radiation (orbital) and all three factors combined (all) on potential evapotranspiration. The present-day MAP for the region is shown with a red dot. (For interpretation of the references to colour in this figure legend, the reader is referred to the web version of this article.)

of future climate and its impacts on vegetation. Inferences of globally increasing drylands as a consequence of future climate change, based on projected decreases in MI (e.g. Huang et al., 2016), substantially overstate present and future drought effects on vegetation (Roderick et al., 2015; Gonsamo et al., 2021). In doing so, they also deviate from the actual projections of future vegetation made by coupled Earth System models that incorporate the positive effect of elevated CO_2 on plant water use efficiency (Greve et al., 2019).

In this paper we have tackled the inverse problem posed by statistical reconstructions of past MI from observed changes in pollen spectra, which neglect the negative effect of low CO_2 on plant water use efficiency and therefore overestimate the dryness of glacial intervals (Chevalier et al., 2020). The method presented here represents a conceptual and practical improvement on the prototype method introduced by Prentice et al. (2017) and applied by Wei et al. (2021). The underlying principle is the same (it relies on the hypothesis that vegetation structure and composition respond to changes in *e*, the ratio of water loss to CO_2 uptake) but it differs from the prototype in the following ways. (1) It is conceptually simpler (contrast Fig. 1 with the equivalent Figure in Prentice et al., 2017), due to its use of vpd as a key intermediate variable (the previous method used the difference between actual and potential evapotranspiration as a proxy); this makes the new method both computationally more straightforward, and easier to understand. (2) The only empirical relationship used (between MI and vpd) is based on an analysis of global data. We also provide a method to infer past mean annual precipitation from the corrected MI, using the well-established set of algorithms implemented in the SPLASH program (Davis et al., 2017) and a further empirical relationship (between MI and cloud cover), also based on a global data analysis.

In common with the method of Prentice et al. (2017), the new method assumes that the palaeotemperature reconstruction is accurate, and not influenced by the CO_2 level. This may be a simplification, as leaf-level temperature responses of photosynthesis are modified by CO_2. However, temperature responses are subject to strong acclimation, and there is no clear experimental evidence for an interaction of CO_2 and temperature effects at the whole-canopy scale (Baig et al., 2015). We conclude that there is currently no basis for assuming any systematic effect of CO_2 on palaeotemperatures reconstructed from pollen data. Any such effect would in any case have only a minor influence on the CO_2-correction of MI, as noted previously.

MI is a useful metric to describe geographic variations in plant-available moisture, but the correct interpretation of absolute values of MI in terms of vegetation structure and function is dependent on the CO_2 level. We have provided a generic method for correcting pollen-based reconstructions that takes this effect into account. It has also been shown that CO_2 has a major effect on future projections of species distribution, which conventional species distribution models (SDMs) ignore (Keenan et al., 2011). The method proposed here would be equally applicable as a method to correct SDM projections in which MI is used as a metric of plant-available moisture (e.g. Porfirio et al., 2014).

The qualitative features of our estimation of hydroclimatic changes at our test site are similar to those previously published (Wei et al., 2021), although the magnitudes of the correction to MI are somewhat smaller. The glacial period, particularly intervals of lowest CO_2, are estimated to have been substantially wetter (in terms of both MI and mean annual precipitation) than the pollen data suggest. At a global scale, consideration of the effects of low CO_2 on vegetation during glacial intervals resolves discrepancies in regions where pollen data appear to show aridity alongside independent evidence of an active hydrological cycle, such as geomorphic evidence for high lake levels and river flows in southern Europe (Moreno et al., 2012) and southeastern Australia (Prentice et al., 2017).

The method described here has been derived partly from first principles and partly from empirical analysis. Ideally it should be subjected to independent, quantitative tests, but devising such tests is a challenge. Palaeohydrological data are rarely sufficiently quantitative for this purpose. One possible (indirect) approach would be via simulations of glacial intervals with Earth System models that include CO_2 effects on

plants through their dynamic vegetation component; however, current models disagree in their simulations of glacial vegetation patterns, potentially adding large uncertainty to any such comparison. This is a topic for further research. There are further uncertain aspects of the model. For example, the assumption of constant β in eq. (7) does not take account of recent evidence for additional effects of aridity (mediated by soil moisture) in modifying β (Lavergne et al., 2020b). The adoption of the method presented here should nonetheless help to mitigate the bias in reconstructed hydroclimates that is inevitably present when the physiological effects of CO_2 on plants are neglected.

Data and code availability

All data used in these analyses are publicly available. For the pollen data from El Cañizar de Villarquemado, see Harrison et al. (2019). For the SMPDS, see Harrison et al. (2019). Equations and code are given in the Appendices and Supplementary Data. The code is archived at: https://zenodo.org/record/5822550#.YiTV2-7P3OQ

Declaration of Competing Interest

The authors declare that they have no known competing financial interests or personal relationships that could have appeared to influence the work reported in this paper.

Acknowledgements

This research has received funding from the European Research Council (ERC) under the European Union's Horizon 2020 research and innovation programme. ICP acknowledges support from the ERC project REALM (Re-inventing ecosystem and land-surface models, grant number 787203). RV-D and SPH acknowledge support from the ERC project GC2.0 (Global Change 2.0: Unlocking the past for a clearer future, grant number 694481).

Appendix 1: An empirical function relating mean growing-season vapour pressure deficit (*D*) to moisture index (MI) and mean growing-season temperature (*T*)

Modern monthly time series climate data at 0.5° resolution from CRU TS 4.04 (Harris et al., 2020) were used to create a climatology for 1961–1990. This was then used to derive daily values of mean growing-season vapour pressure deficit (*D*), moisture index (MI) and mean growing-season temperature (*T*) using mean-preserving autoregressive interpolation (Rymes and Myers, 2001). The growing season was conventionally defined as days when the air temperature was >0 °C; although the threshold for growth of most plants is somewhat above 0 °C (often around 5 °C), this definition allows for the fact that leaf temperatures in plants of cold climates, especially herbaceous plants, are commonly higher than air temperatures during daytime. The empirical relationship between *D*, MI and *T* was fitted only for temperatures >5 °C, however, because locations with mean growing-season temperature below 5 °C are often unvegetated, and showed erratic variation in *D*. The relationship was fitted by non-linear regression using an exponential function as follows:

$$D = a\, exp.[(b\, T) - (c\, \mathrm{MI})\,] \quad \text{(A1.1)}$$

The final fitted function is given by:

$$\mathrm{D} = 4.612324{*}exp.(0.060925{*}\mathrm{T} - 0.872589{*}\mathrm{MI})\ [\mathrm{hPa}] \quad \text{(A1.2)}$$

Plot showing the relationship between vapour pressure deficit (D) and moisture index (MI) at different temperatures. The black dotted lines are the predictions for the mid-point of each temperature class.

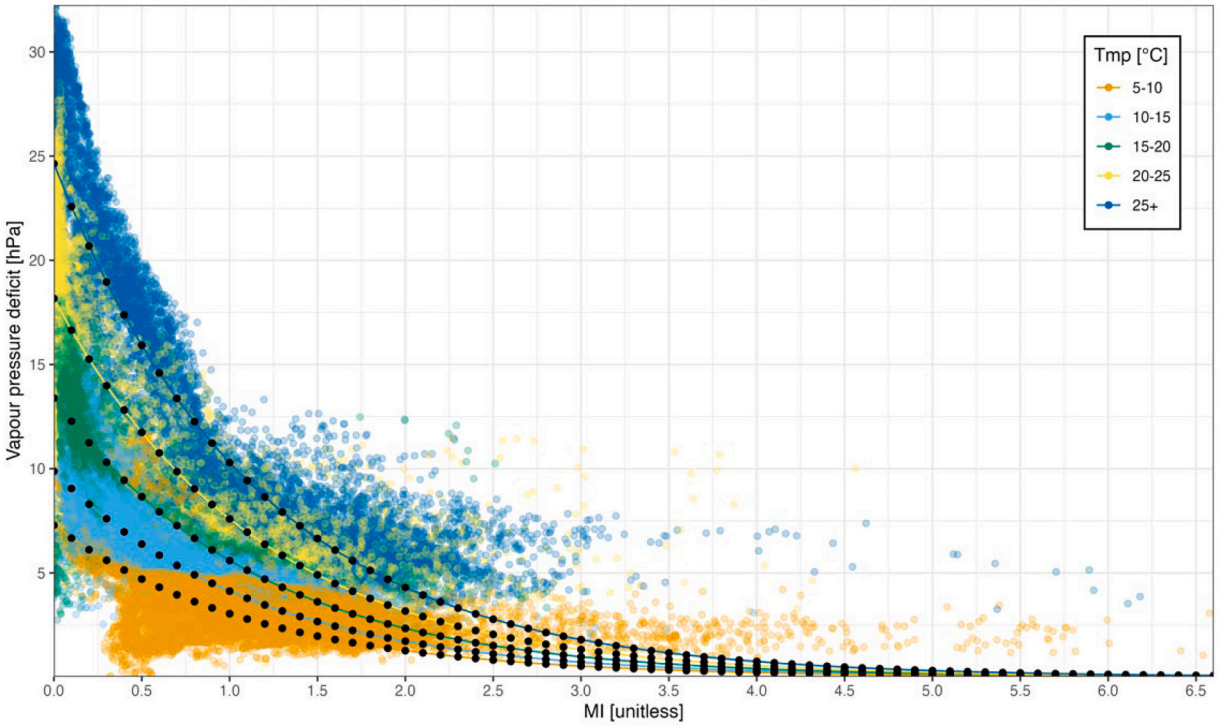

References

Harris, I.C.; Jones, P.D.; Osborn, T. (2020): CRU TS4.04: Climatic Research Unit (CRU) Time-Series (TS) version 4.04 of high-resolution gridded data of month-by-month variation in climate (Jan. 1901- Dec. 2019). Centre for Environmental Data Analysis, date of citation. https://catalogue.ceda.ac.uk/uuid/89e1e34ec3554dc98594a5732622bce9

Rymes, M.D. and Myers, D.R., 2001. Mean preserving algorithm for smoothly interpolating averaged data. Sol. Energy, 71(4), pp.225–231. DOI/URL: doi:https://doi.org/10.1016/S0038-092X(01)00052-4.

Appendix 2: The response of the ratio of leaf-internal to ambient CO_2 (χ) to changes in ambient CO_2 partial pressure (c_a), based on experiments by Schubert and Jahren (2012)

Equation (4) in Schubert and Jahren (2012) describes the hyperbolic response of stable carbon isotope discrimination (Δ) of above-ground plant tissues to variation in c_a, expressed in parts per million (ppm, equivalent to μmol mol^{-1}):

$$\Delta = b\, m\, (c_a + c_0)/\{b + m\, (c_a + c_0)\} \quad \text{(A2.1)}$$

based on the common response shown in experiments on two C_3 plant species, with all environmental variables apart from c_a held constant. The estimated values of the constants are b = 28.26‰, m = 0.35‰ ppm^{-1} and c_0 = 15 ppm. Δ is related to χ by the standard equation relating discrimination and χ:

$$\chi = (\Delta - a)/(b - a) \quad \text{(A2.2)}$$

where a = 4.4‰. Substituting (A2.2) into (A2.1) yields:

$$\chi = (c_a + q)/\{c_a + (b/m + c_0)\} \quad \text{(A2.3)}$$

where q is a composite term that is constrained to equal zero. Hence,

$$\chi = c_a/(c_a + 95.7) \quad \text{(A2.4)}$$

where the constant in the denominator has units of ppm, and is equivalent to 9.7 Pa at sea level.

Appendix 3: An empirical function relating fractional cloud cover (cld) to moisture index (MI).

Modern monthly time series climate data at 0.5° resolution from CRU TS 4.04 (Harris et al., 2020) were used to create a climatology for 1961–1990. This was then used to derive daily values of fractional cloud cover (cld) and moisture index (MI) using mean-preserving autoregressive interpolation (Rymes and Myers, 2001). The growing season was defined as days when the air temperature was >0 °C. The empirical relationship between cld and MI and was fitted for temperatures >0 °C by non-linear regression using an exponential function as follows:

$$\text{cld} = a + b\, [1 - exp.(-\text{c MI})] \quad \text{(A3.1)}$$

The final fitted function is given by:

$$\text{cld} = 28.00680 + 45.17031*(1 - exp.(-1.83127*\text{MI})) \quad \text{(A3.2)}$$

Plot showing the relationship between cloud cover and MI.

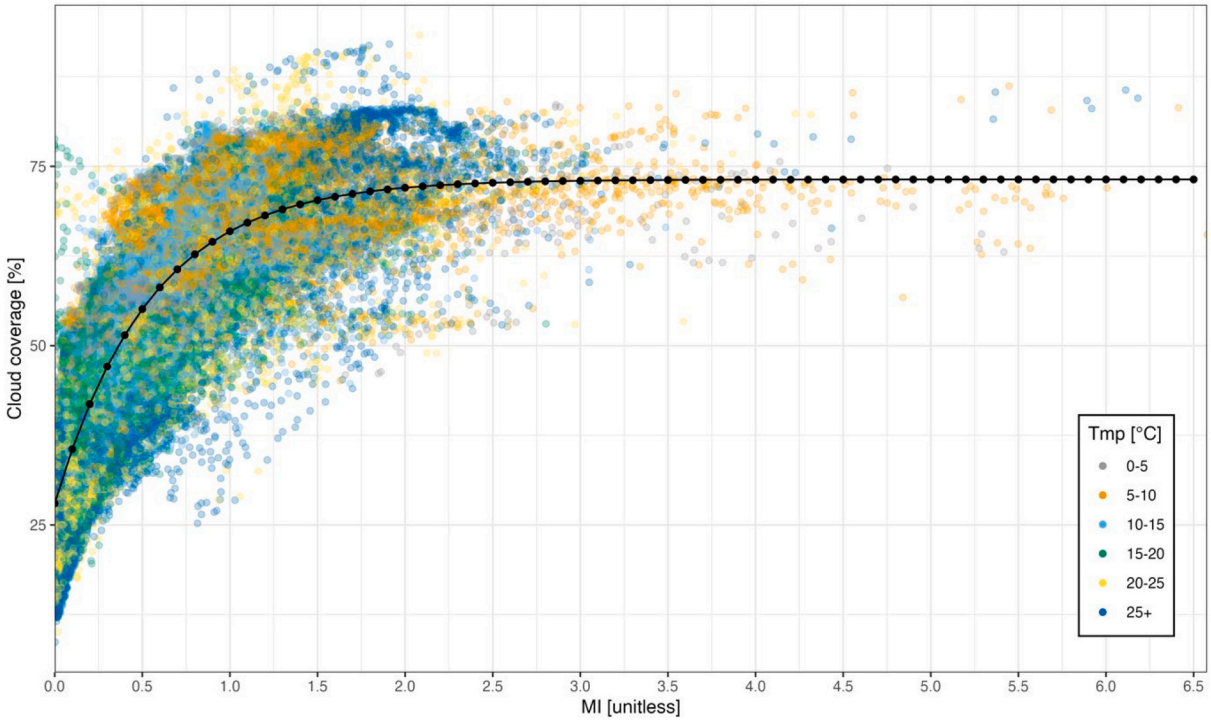

References

Harris, I.C.; Jones, P.D.; Osborn, T. (2020): CRU TS4.04: Climatic Research Unit (CRU) Time-Series (TS) version 4.04 of high-resolution gridded data of month-by-month variation in climate (Jan. 1901- Dec. 2019). Centre for Environmental Data Analysis, date of citation. https://catalogue.ceda.ac.uk/uuid/89e1e34ec3554dc98594a5732622bce9

Rymes, M.D. and Myers, D.R., 2001. Mean preserving algorithm for smoothly interpolating averaged data. Sol. Energy, 71(4), pp.225–231. DOI/URL: doi:https://doi.org/10.1016/S0038-092X(01)00052-4.

Appendix A. Supplementary data

Supplementary data to this article can be found online at https://doi.org/10.1016/j.gloplacha.2022.103790.

References

Archer, S.R., Andersen, E.M., Predick, K.I., Schwinning, S., Steidl, R.J., Woods, S.R., 2017. Woody plant encroachment: Causes and consequences. In: Briske, D. (Ed.), Rangeland Systems. Springer Series on Environmental Management. Springer, Cham. https://doi.org/10.1007/978-3-319-46709-2_2.

Arora, V., Katavouta, A., Williams, R.G., Jones, C.D., Brovkin, V., Friedlingstein, P., Schwinger, J., Bopp, L., Boucher, O., Cadule, P., Chamberlain, M.A., Christian, J.R., Delire, C., Fisher, R.A., Hajima, T., Ilyina, T., Joetzjer, E., Kawamiya, M., Koven, C. D., Krasting, J.P., Law, R.M., Lawrence, D.M., Lenton, A., Lindsay, K., Pongratz, J., Raddatz, T., Séférian, R., Tachiiri, K., Tjiputra, J.F., Wiltshire, A., Wu, T., Ziehn, T., 2020. Carbon–concentration and carbon–climate feedbacks in CMIP6 models and their comparison to CMIP5 models. Biogeosci. 17, 4173–4222. https://doi.org/10.5194/bg-17-4173-2020.

Baig, S., Medlyn, B.E., Mercado, L.M., Zaehle, S., 2015. Does the growth response of woody plants to elevated CO_2 increase with temperature? A model-oriented meta-analysis. Glob. Chang. Biol. 21, 4303–4319. https://doi.org/10.1111/gcb.12962.

Bragg, F.J., Prentice, I.C., Harrison, S.P., Eglinton, G., Foster, P.N., Rommerskirchen, F., Rullkötter, J., 2013. Stable isotope and modelling evidence for CO_2 as a driver of glacial-interglacial vegetation shifts in southern Africa. Biogeosci. 10, 2001–2010.

Chevalier, M., Davis, B.A.S., Heiri, O., Seppä, H., Chase, B.M., Gajewski, K., Lacourse, T., Telford, R.J., Finsinger, W., Guiot, J., Kühl, N., Maezumi, S.Y., Tipton, J.R., Carter, V.A., Brussel, T., Phelps, L.N., Dawson, A., Zanon, M., Vallé, F., Nolan, C., Mauri, A., de Vernal, A., Izumi, K., Holmström, L., Marsicek, J., Goring, S., Sommer, P.S., Chaput, N., Kupriyanov, D., 2020. Pollen-based climate reconstruction techniques for late Quaternary studies. Earth Sci. Rev. 210, 103384.

Cleator, S.F., Harrison, S.P., Nichols, N.K., Prentice, I.C., Roustone, I., 2020. A new multivariable benchmark for last Glacial Maximum climate simulations. Clim. Past 16, 699–712. https://doi.org/10.5194/cp-16-699-2020.

Cowling, S.A., Sykes, M.T., 1999. Physiological significance of low atmospheric CO_2 for plant-climate interactions. Quat. Res. 52, 237–242.

Davis, T.W., Prentice, I.C., Stocker, B.D., Thomas, R.T., Whitley, R.J., Wang, H., Evans, B. J., Gallego-Sala, A.V., Sykes, M.T., Cramer, W., 2017. Simple process-led algorithms for simulating habitats (SPLASH v.1.0): robust indices of radiation, evapotranspiration and plant-available moisture. Geosci. Model Dev. 10, 689–708.

Dekker, S.C., Groenendijk, M., Booth, B.B.B., Huntingford, C., Cox, P.M., 2016. Spatial and temporal variations in plant water use efficiency inferred from tree-ring, eddy covariance and atmospheric observations. Earth Syst. Dynam. 7, 525–533.

Eamus, D., Palmer, A.R., 2007. Is climate change a possible explanation for woody thickening in arid and semi-arid regions? Res Letters Ecol. https://doi.org/10.1155/2007/37364.

Farquhar, G.D., 1997. Carbon dioxide and vegetation. Science 278, 1411.

Friedlingstein, P., Jones, M.W., O'Sullivan, M., Andrew, R.M., Hauck, J., Peters, G.P., Peters, W., Pongratz, J., Sitch, S., Le Quéré, C., Bakker, D.C.E., Canadell, J.G., Ciais, P., Jackson, R.B., Anthoni, P., Barbero, L., Bastos, A., Bastrikov, V., Becker, M., Bopp, L., Buitenhuis, E., Chandra, N., Chevallier, F., Chini, L.P., Currie, K.I., Feely, R. A., Gehlen, M., Gilfillan, D., Gkritzalis, T., Goll, D.S., Gruber, N., Gutekunst, S., Harris, I., Haverd, V., Houghton, R.A., Hurtt, G., Ilyina, T., Jain, A.K., Joetzjer, E., Kaplan, J.O., Kato, E., Klein Goldewijk, K., Korsbakken, J.I., Landschützer, P., Lauvset, S.K., Lefèvre, N., Lenton, A., Lienert, S., Lombardozzi, D., Marland, G., McGuire, P.C., Melton, J.R., Metzl, N., Munro, D.R., Nabel, J.E.M.S., Nakaoka, S.-I., Neill, C., Omar, A.M., Ono, T., Peregon, A., Pierrot, D., Poulter, B., Rehder, G., Resplandy, L., Robertson, E., Rödenbeck, C., Séférian, R., Schwinger, J., Smith, N., Tans, P.P., Tian, H., Tilbrook, B., Tubiello, F.N., van der Werf, G.R., Wiltshire, A.J., Zaehle, S., 2019. Global carbon budget 2019. Earth Syst. Sci. Data 11, 1783–1838. https://doi.org/10.5194/essd-11-1783-2019.

Garreta, V., Guiot, J., Mortier, F., Chadœuf, J., Hély, C., 2012. Pollen-based climate reconstruction: Calibration of the vegetation–pollen processes. Ecol. Model. 235-236, 81–94. https://doi.org/10.1016/j.ecolmodel.2012.03.031.

Garreta, V., Miller, P.A., Guiot, J., Hély, C., Brewer, S., Sykes, M.T., Litt, T., 2010. A method for climate and vegetation reconstruction through the inversion of a dynamic vegetation model. Clim. Dyn. 35, 371–389.

Gonsamo, A., Ciais, P., Miralles, D.G., Sitch, S., Dorigo, W., Lombardozzi, D., Friedlingstein, P., Nable, J.E.M.S., Goll, D.S., O'Sullivan, M., Arneth, A., Anthoni, P., Jain, A.K., Wiltshire, A., Peylin, P., Cescatti, A., 2021. Greening drylands despite warming consistent with carbon dioxide fertilization effect. Glob. Chang. Biol. 27, 3336–3349. https://doi.org/10.1111/gcb.15658.

González-Sampériz, P., Gil-Romera, G., García-Prieto, E., Aranbarri, J., Moreno, A., Morellón, M., Sevilla-Callejo, M., Leunda, M., Santos, L., Franco-Múgica, F., Andrade, A., Carrión, J.S., Valero-Garcés, B.L., 2020. Strong continentality and effective moisture drove unforeseen vegetation dynamics since the last interglacial at inland Mediterranean areas: the Villarquemado sequence in NE Iberia. Quat. Sci. Rev. 242, 106425 https://doi.org/10.1016/j.quascirev.2020.106425.

Greve, P., Roderick, M.L., Ukkola, A.M., Wada, Y., 2019. The aridity Index under global warming. Environ. Res. Lett. 14, 124006 https://doi.org/10.1088/1748-9326/ab5046.

Guiot, J., Torre, F., Jolly, D., Peyron, O., Boreux, J.J., Cheddadi, R., 2000. Inverse vegetation modeling by Monte Carlo sampling to reconstruct palaeoclimates under changed precipitation seasonality and CO_2 conditions: application to glacial climate in Mediterranean region. Ecol. Model. 127, 119–140.

Harrison, S.P., 2019. Modern pollen data for climate reconstructions, version 1 (SMPDS). University of Reading. 10.17864/1947.194.

Harrison, S.P., Prentice, I.C., 2003. Climate and CO_2 controls on global vegetation distribution at the last Glacial Maximum: analysis based on palaeovegetation data, biome modelling and palaeoclimate simulations. Glob. Chang. Biol. 9, 983–1004.

Harrison, S.P., González-Sampériz, P., Gil-Romera, G., 2019. Fossil pollen data for climate reconstructions from El Cañizar de Villarquemado. University of Reading. 10.17864/1947.219.

Haverd, V., Smith, B., Canadell, J.G., Cuntz, M., Mikaloff-Fletcher, S., Farquhar, G., Woodgate, W., Briggs, P.R., Trudinger, C.M., 2020. Higher than expected CO_2 fertilization inferred from leaf to global observations. Glob. Chang. Biol. 26, 2390–2402. https://doi.org/10.1111/gcb.14950.

Haxeltine, A., Prentice, I.C., 1996. BIOME3: an equilibrium terrestrial biosphere model based on ecophysiological constraints, resource availability, and competition among plant functional types. Glob. Biogeochem. Cycles 10, 693–709. https://doi.org/10.1029/96GB02344.

Huang, J., Yu, H., Guan, X., Wang, G., Guo, R., 2016. Accelerated dryland expansion under climate change. Nat. Clim. Chang. 6, 166–171. https://doi.org/10.1038/nclimate2837.

Idso, S.B., 1989. A problem for paleoclimatology? Quat. Res. 31, 433–434.

Izumi, K., Bartlein, P.J., 2016. North American paleoclimate reconstructions for the last Glacial Maximum using an inverse modeling through iterative forward modeling approach applied to pollen data. Geophys. Res. Lett. 43, 10965–10972.

Jolly, D., Haxeltine, A., 1997. Effect of low glacial atmospheric CO_2 on tropical African montane vegetation. Science 276, 786–788.

Kaplan, J.O., Bigelow, N.H., Bartlein, P.J., Christensen, T.R., Cramer, W., Harrison, S.P., Matveyeva, N.V., McGuire, A.D., Murray, D.F., Prentice, I.C., Razzhivin, V.Y., Smith, B., Walker, D.A., Anderson, P.M., Andreev, A.A., Brubaker, L.B., Ed.wards, M. E., Lozhkin, A.V., 2003. Climate change and Arctic ecosystems: 2. Modeling, paleodata-model comparisons, and future projections. J. Geophys. Res. 108 (D19), 8171. https://doi.org/10.1029/2002JD002559.

Keenan, T., Serra-Diaz, J.M., Lloret, F., Ninyerola, M., Sabaté, S., 2011. Predicting the future of forests in the Mediterranean under climate change, with niche- and process-based models: CO_2 matters! Glob. Chang. Biol. 17, 565–579.

Keenan, T.F., Hollinger, D.Y., Bohrer, G., Dragoni, D., Munger, J.W., Schmid, H.P., Richardson, A.D., 2013. Increase in forest water-use efficiency as atmospheric carbon dioxide concentrations rise. Nature 499, 324–327.

Lavergne, A., Voelker, S., Csank, A., Graven, H., de Boer, H.J., Daux, V., Robertson, I., Dorado-Liñá, I., Martínez-Sancho, E., Battipaglia, G., Bloomfield, K.J., Still, C.J., Meinzer, F.C., Dawson, T.E., Camarero, J.J., Clisby, R., Fang, Y., Menzel, A., Keen, R. M., Roden, J.S., Prentice, I.C., 2020a. Historical changes in the stomatal limitation of photosynthesis: empirical support for an optimality principle. New Phytol. 225, 2484–2497.

Lavergne, A., Sandoval, D., Hare, V.J., Graven, H., Prentice, I.C., 2020b. Impacts of soil water stress on the acclimated stomatal limitation of photosynthesis: insights from stable carbon isotope data. Glob. Chang. Biol. 26, 7158–7172.

Liu, M., Prentice, I.C., Ter Braak, C.J.F., Harrison, S.P., 2020. An improved statistical approach for reconstructing past climates from biotic assemblages. Proc. Roy. Soc. A, Mathematics A 476, 20200346. https://doi.org/10.1098/rspa.2020.0346.

Martin Calvo, M., Prentice, I.C., 2015. Effects of fire and CO_2 on biogeography and primary production in glacial and modern climates. New Phytol. 208, 987–994.

Moreno, A., González-Sampériz, P., Morellón, M., Valero-Garcés, B.L., Fletcher, W.J., 2012. Northern Iberian abrupt climate change dynamics during the last glacial cycle: a view from lacustrine sediments. Quat. Sci. Rev. 36, 139–153. https://doi.org/10.1016/j.quascirev.2010.06.031.

Piao, S., Friedlingstein, P., Ciais, P., Zhou, L., Chen, A., 2006. Effect of climate and CO_2 changes on the greening of the Northern Hemisphere over the past two decades. Geophys. Res. Lett. 33, L23402. https://doi.org/10.1029/2006GL028205.

Polley, H.W., Johnson, H.B., Marino, B.D., Mayeux, H.S., 1993. Increases in C_3 plant water-use efficiency and biomass over glacial to present CO_2 concentrations. Nature 361, 61–64.

Porfirio, L.L., Harris, R.M.B., Lefroy, E.C., Hugh, S., Gould, S.F., Lee, G., Bindoff, N.L., Mackey, B., 2014. Improving the use of species distribution models in conservation planning and management under climate change. PLoS One 9, e113749. https://doi.org/10.1371/journal.pone.0113749.

Prentice, I.C., Harrison, S.P., Bartlein, P.J., 2011. Global vegetation and terrestrial carbon cycle changes after the last ice age. New Phytol. 189, 988–998.

Prentice, I.C., Dong, N., Gleason, S.M., Maire, V., Wright, I.J., 2014. Balancing the costs of carbon gain and water loss: testing a new quantitative framework for plant functional ecology. Ecol. Lett. 17, 82–91.

Prentice, I.C., Cleator, S.F., Huang, Y.F., Harrison, S.P., Roulstone, I., 2017. Reconstructing ice -age climates: quantifying low-CO_2 effects on plants. Glob. Planet. Chang. 149, 166–176. https://doi.org/10.1016/j.gloplacha.2016.12.012.

Roderick, M.L., Greve, P., Farquhar, G.D., 2015. On the assessment of aridity with changes in atmospheric CO_2. Water Resour. Res. 51, 5450–5463. https://doi.org/10.1002/2015WR017031.

Schubert, B.A., Jahren, A.H., 2012. The effect of atmospheric CO_2 concentration on carbon isotope fractionation in C_3 land plants. Geochim. Cosmochim. Acta 96, 29–43.

Schubert, B.A., Jahren, A.H., 2015. Global increase in plant carbon isotope fractionation following the last Glacial Maximum caused by increase in atmospheric pCO_2. Geology 43, 435–438. https://doi.org/10.1130/G36467.1.

Solomon, A.M., 1984. Forest responses to complex interacting fullglacial environmental conditions. AMQUA Abstracts 8, 120.

Stocker, B.D., Wang, H., Smith, N.G., Harrison, S.P., Keenan, T.F., Sandoval, D., Davis, T., Prentice, I.C., 2020. P-model v1.0: an optimality-based light use efficiency model for simulating ecosystem gross primary production. Geosci. Model Dev. 13, 1545–1581.

Valero-Garcés, B.L., González-Sampériz, P., Gil-Romera, G., Benito, B., Moreno, A., Oliva-Urcia, B., Aranbarri, J., García-Prieto, E., Frugone, M., Morellón, M., Arnold, L. J., Demuro, M., Hardiman, M., Blockley, S.P.E., Lane, C.S., 2019. A multi-dating approach to age-modelling long continental records: the 135 ka El Cañizar de Villarquemado sequence (NE Spain). Quat. Geochronol. 54, 101006 https://doi.org/10.1016/j.quageo.2019.101006.

Voelker, S.L., Brooks, J.R., Meinzer, F.C., Anderson, R., Bader, M.K.-F., Battipaglia, G., Becklin, K.M., Beerling, D., Bert, D., Betancourt, J.L., Dawson, T.E., Domec, J.-C., Guyette, R.P., Körner, C., Leavitt, S.W., Linder, S., Marshall, J.D., Mildner, M., Ogée, J., Panyushkina, I., Plumpton, H.J., Pregitzer, K.S., Saurer, M., Smith, A.R., Siegwolf, R.T.W., Stambaugh, M.C., Talhelm, A.F., Tardif, J.C., Van de Water, P.K., Ward, J.K., Wingate, L., 2016. A dynamic leaf gas-exchange strategy is conserved in woody plants under changing ambient CO_2: evidence from carbon isotope discrimination in paleo and CO_2 enrichment studies. Glob. Chang. Biol. 22, 889–902. https://doi.org/10.1111/gcb.13102.

Wang, H., Prentice, I.C., Cornwell, W.M., Keenan, T.F., Davis, T.W., Wright, I.J., Evans, B.J., Peng, C., 2017. Towards a universal model for carbon dioxide uptake by plants. Nature Plants 3, 734–741.

Wei, D., González-Sampériz, P., Gil-Romera, G., Harrison, S.P., Prentice, I.C., 2021. Seasonal temperature and moisture changes in interior semi-arid Spain from the last interglacial to the late Holocene. Quat. Res. 101, 143–155. https://doi.org/10.1017/qua.2020.108.

Wu, H., Guiot, J., Brewer, S.C., Guo, Z.T., 2007. Climatic changes in Eurasia and Africa at the last glacial maximum and mid-Holocene: reconstruction from pollen data using inverse vegetation modelling. Clim. Dyn. 29, 211–229.

Zhu, Z., Piao, S., Myneni, R., Huang, M., Zeng, Z., Canadell, J.G., Ciais, P., Sitch, S., Friedlingstein, P., Arneth, A., Cao, C., Cheng, L., Kato, E., Koven, C., Li, Y., Lian, X., Liu, Y., Liu, R., Mao, J., Pan, Y., Peng, S., Peñuelas, J., Poulter, B., Pugh, T.A.M., Stocker, B.D., Viovy, N., Wang, X., Wang, Y., Xiao, Z., Yang, H., Zaehle, S., Zeng, N., 2016. Greening of the Earth and its drivers. Nat. Clim. Chang. 6, 791–795. https://doi.org/10.1038/nclimate3004.